https://dx.doi.org/10.4314/dujopas.v9i4a.17
ISSN (Print): 2476-8316
ISSN (Online): 2635-3490
Dutse Journal of Pure and Applied Sciences (DUJOPAS), *Vol. 9 No. 4a December 2023*

Magnetic Structural Depth Classification Using Center for Exploration Targeting And 3D Euler Deconvolution: A Case Study of Shanga (Sheet 96) North West, Nigeria

[1*]Mam Daniel Tawey, [2] Ayamezimi Oziofu Ehinlaiye, [1]Ibrahim Abdulrazaq Adesoji

[1]National Water Resources Institute,
Mando Road,
Kaduna
Nigeria

[2]Geology Department,
University of Benin

Email: taweymam@gmail.com

Abstract

The present study involved the use of 3D Euler deconvolution to classify the depth of occurrences of magnetic structures as explicated and elucidated by the Centre for Exploration Targeting Plug-in (CET). To achieve this aim, the residual magnetic anomaly was first reduced to the equator (RTE) to centre the anomaly peaks directly above each causative source. After that, the RTE data was imputed into the CET plug-in, which is an extension of Oasis Montaj, to delineate structures that occur within the area. A 3D Euler deconvolution map with a structural index of one (SI = 1) that identified faults, dykes, and horizontal bodies was created using the RTE data. The Euler deconvolution depths were classified for depths that are <150 m, between 150 m and 300 m, 300 m and 450 m, and > 450 m. The CET delineated structures were superimposed over the 3D Euler deconvolution map with SI = 1, and most of the CET structures coincided with the structures from the Euler deconvolution map with SI = 1. Since Euler solutions are classified based on depth, the Euler structural map was used to classify the CET delineated structures based on their depths. The Euler structural map was imported into ArcGIS version 10.8 to digitize the structures based on their corresponding depth as displayed on the 3D Euler deconvolution map of SI = 1. After digitizing the Euler map with a structural index equal to one (SI = 1) with classified depth, a new structural map was then produced depicting each structure delineated with the CET based on their respective depth.

Keywords: Depth, 3D Euler, CET, Structures, RTE

INTRODUCTION

The occurrence of magnetic source edges (structural lineaments) and their depth can be estimated by employing many source edge detection methods by doing a structural analysis of the aeromagnetic data. In general, derivatives are highly helpful in structural delineation of magnetic source bodies. These source edge detection methods include: First and second vertical derivatives (FVD and SVD) that are used to delineate faults and linear features (Foss, 2011; Gunn *et al.,* 1997), by using the Horizontal Gradient Magnitude (HGM) approach, it is possible to map linear structures from potential field data, like the fault zones and/or dykes.(Phillips, 2000; Grauch and Cordell, 1987) and the analytical signal (AS) is highly

**Author for Correspondence*

susceptible to the edge effects of the causing magnetic bodies since it shares qualities with the magnetic field's derivative properties. (Roest *et al.,* 1992). Also, the Tilt derivative locates the edges of the sources of the TMI anomaly and has the advantage of equalizing the amplitudes of potential field anomalies for short and long wavelengths (Verduzco *et al.,* 2004; Miller & Singh, 1994), the Centre for Exploration Targeting (CET), a collection of algorithms that offer functionality for enhancing field data, detection of geological lineaments with complex structural analysis. All these methods mentioned can only be used to delineate source edges and location (position) of a magnetic body without the Depth of the structures delineated directly but the 3D Euler deconvolution as put forward by (Reid *et al.,* 1990) can evaluate and display edges and depth of a magnetic source at the same time as such, in this study, we have been able to delineate and classify structural lineaments within Shanga using Centre for exploration targeting plug-In CET base on their depth by employing the 3D Euler convolution with structural index of one (SI=1).

Several research have been published employing Euler deconvolution and centre for exploration targeting plug-in CET for structural delineation or its integration with other depth estimation techniques such as analytic signal (AS) depth estimation method, source parameter imaging (SPI) within and outside Nigeria (tawey *et al.,*2020a and 2020b, Andrew *et al.,* 2018)

Location, Tectonic settings, and Geology of the study area

The study area is in the northwest of Nigeria, between Niger and Kebbi states, and bordered by longitude 4^{0} 30" east and longitude 5^{0} 00" east and latitude 11^{0} 00" north and 11^{0} 30" north (Figure. 1). Elevation across the area varies from 132 m low to 349 m high (Figure 2a). The study area is partly Basement to the eastern portion and partly sedimentary to the west (Figures 2a & 2b). The basement complex of Nigeria is tectonically situated in the Pan-African mobile belt between West African and Congo Cratons in the south of the Tuareg Shield (Black, 1980), and it is a

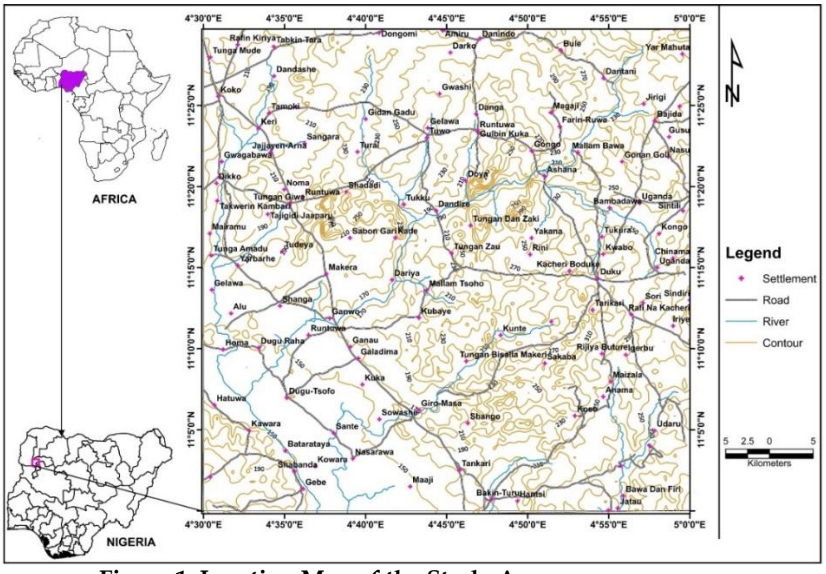

Figure 1: Location Map of the Study Area

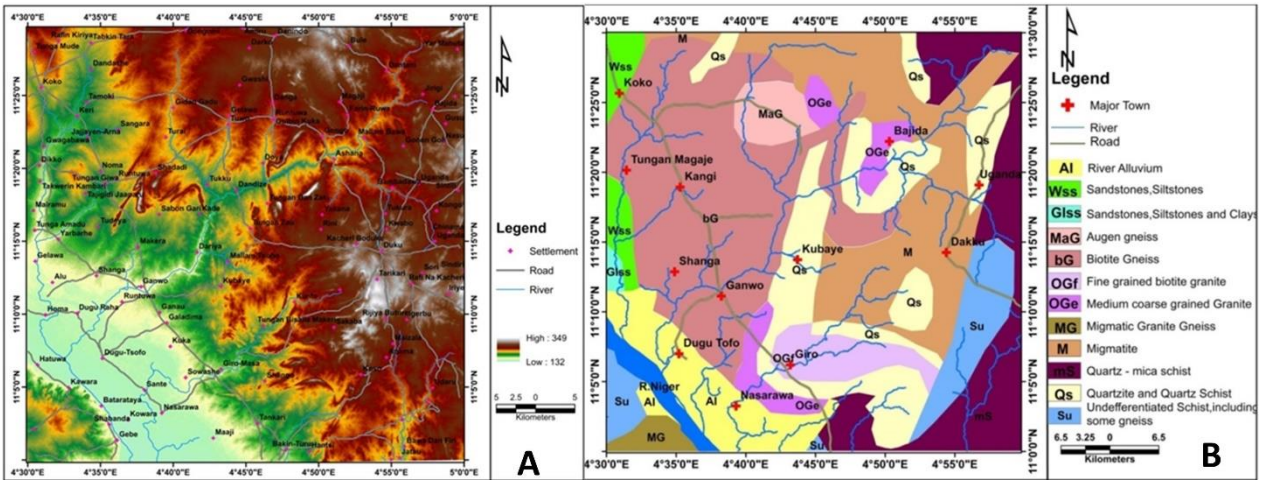

Figure 2: a. DEM showing elevation across the study Area and b. Geologic map of the area (Adapted from NGSA, 2006)

reactivated area formed by plate collision between West African craton and the Pharusian margin (Dada, 2006; Burke & Dewey, 1972).

The basement rocks are characterised to have been emanated because of series of mountain building processes that involved deformation, metamorphism, and remobilization and the last of these episodes is the Pan-African with the widespread development of granites and gneisses during this tectonic period, deformation, large-scale metamorphism, and migmatisation are characteristics of the Pan-African (Abba, 1983). As tectonic activity progressed, contact metamorphism, which came after this last deformation, is thought to have contributed to the creation of granites and granodiorites. Faulting and fracture marked the end of the Pan African orogeny (Olayinka, 1992; Gandu *et al.*, 1986).

The research area is part of Sokoto Basin in Nigeria and an embayment of Iullemeden Basin (Odebode, 2010). The Sokoto Basin has been described to be a young West African inland cratonic sedimentary basin (Obaje, 2009; McCurry, 1976). Faulting activities that caused stabilized crust to extend and experience epeirogeny warping are what gave rise to the Basin. These activities, which started around the early part of the Palaeozoic and persisted throughout the Upper Cretaceous, was largely responsible for the sediments accumulated inside the basin spreading southwest (Kogbe, 1979 and 1981).

In this region, sedimentary rocks are found along the western boundary of the research area and basement rocks to the left flank from the area's centre to the east (Figure 2b).

Source of Aeromagnetic Data

The airborne magnetic data used in this present research is a high-resolution data collected by Fugro Airborne Survey for Nigeria Geologic Survey Agency (NGSA) that covers parts of Nigeria in 2009 in a sequence of northwest to southeast flight lines of magnetic surveys flown at a spacing of 500 m and topographical height of 80 m, and the survey covered 826,000 km.

Methodology

The residual magnetic anomaly data of the study area was reduced to the equator (RTE) to place the anomalies directly above each causative source after that, the RTE data was imputed into the CET plug-in which is an extension of Oasis Montaj, and the structures were delineated. Also, the RTE data was used to generate 3D Euler deconvolution map with SI=1, for fault, Dyke/sill which in theory and practical similar and equivalent to the structural

lineament map produced using CET plug-in and the structures in the 3D Euler deconvolution map were classified based on their respective depths, for structural depths that are less than 150 m, those between 150 m and 300 m, structures at depth of 300 m to 450 m and structures at depths greater than 450 m. CET delineated structures were superimposed on the 3D Euler Deconvolution map with SI=1, in the Arc Map version 10.8 environment to digitised the structures base on their corresponding depth as displayed on Euler deconvolution map (SI=1). After digitizing the CET structural map with classified depths, the CET structural map was then reproduced depicting each structure based on their respective range of depths.

Theory of the Methods

Upward continuation

When upward continuation is applied to airborne magnetic data, the anomalies of shallow features are made to diminished in intensity, while the anomalies of deeper sources are comparatively enhanced. As a result, the technique can be used as a filtering method to separate regional anomaly from residual anomaly (Reynolds, 1997). Whenever anomaly from deep sources is removed from the total field, what is left after the subtraction of the deep source anomaly is called the residual field (Telford *et al.,* 1990). For a total field F (x, y, 0).

$$F(x,y,-h) = \frac{h}{2\pi}\iint \frac{F(x,y,0)\partial x\partial y}{\sqrt{\left(x-x^i\right)^2+\left(y-y^i\right)^2+h^2}} \quad (1)$$

The equation above, when used in conjunction with knowledge of magnetization values over the surface, enables us to determine magnetization anyplace in free space. The total field at the known surface F (x, y, 0) at point P (x, y, -h) is shown on the left side. The residual data were separated from the regional data for the research area using the upward continuation method.

Reduction to magnetic equator

With the assumption that all magnetic fields seen in the study region are the result of induced magnetic effects, the reduced to equator (RTE) technique aims to create a magnetic map equivalent to what would have been obtained if the area had been surveyed at the magnetic equator. Data that was collected while the earth's magnetic field was inclined is transformed into data that would have been collected while the magnetic field was vertical by this filter. The anomalies are centered over potions where their sources are located using this technique at low magnetic latitudes. This technique can simplify data interpretation without sacrificing its geophysical significance. We use the equation below for RTE transformation.

$$L(\theta) = \frac{[\sin(I)-i.\cos(I).\cos(D-\theta)]^2 X(-\cos^2(D-\theta))}{[Sin^2\,(I_a)+\mathrm{Cos}^2\,(I_a).\mathrm{Cos}^2\,(D-\theta)]X[Sin^2\,(I)+\mathrm{Cos}^2\,(I).\mathrm{Cos}^2\,(D-\theta)]} \quad \text{if}(\setminus I_a \setminus) < (\setminus I \setminus), I_a = 1 \ (2)$$

Where I represent the geomagnetic inclination, I_a is the inclination for amplitude correction, *D* represents the geomagnetic declination, Sin (*I*) is the amplitude component while *i*cos(*I*)cos(D-θ) is the phase component.

Centre for exploration targeting (CET) for structures.

The CET is a collection of algorithms that provide capabilities for improving, identifying lineaments, and analysing the structural complexity of potential field data (Holden *et al.,* 2008; Core *et al.,* 2009). Utilizing the total magnetic intensity, the method uses automated delineation of geologic structures to identify potential mineral deposit locations.

It uses statistical steps like analysis of texture, delineation of lineation, vectorisation, and complexity analysis for contact occurrences (Geosoft, 2012).

The CET method enhances magnetic data by discovering discontinuity zones and irregularities, spotting and detecting structures, and abruption in intensity utilizing symmetry axes. Magnetic discontinuity in an area involves rock edges, elongated structures, and intrusions, affecting geologic framework (Kovesi, 1991). By using texture amplification, regions of magnetic discontinuity are portrayed as skeletal structures.

3D Euler deconvolution

Euler deconvolution can be applied in the estimation of depth of an anomaly within a grid and can also be used to proffer a border between two lithology within the grid (Reid *et al.*,1990). It uses the homogeneity connection presented by Thompson to retrieve information from grids (1982). The following expression can be used to express this connection:

$$(x - x_0)\frac{\delta T}{\delta x} + (y - y_0)\frac{\delta T}{\delta y} + (z - z_0)\frac{\delta T}{\delta z} = N(B - T) \quad (3)$$

Where $(x_{0,}\, y_0\, z_0)$ is a magnetic source's location, and T is the total field that was observed at (x, y, z). N is the value of the structural index (SI), that represents the rate of increase or decrease at field distance. The structural index can be chosen if the source's geometry is known in advance while B represents the regional field value.

Results and Discussion

Figure 3a represents the total field map while Figure 4b represents the RMI map, Figure 4c represent the (RTE) and Figure 4d represent the structural map of the area delineated from CET. From Figure 4a, the susceptibility varies between 33000.7 nT low to 33200.5 nT. High susceptibility values are confined to the southwestern side of the map while low susceptibility values are confined to the northwest and southcentral portion of the map with alternating occurrences of magnetic lows and highs. On Figure 4b, susceptibility

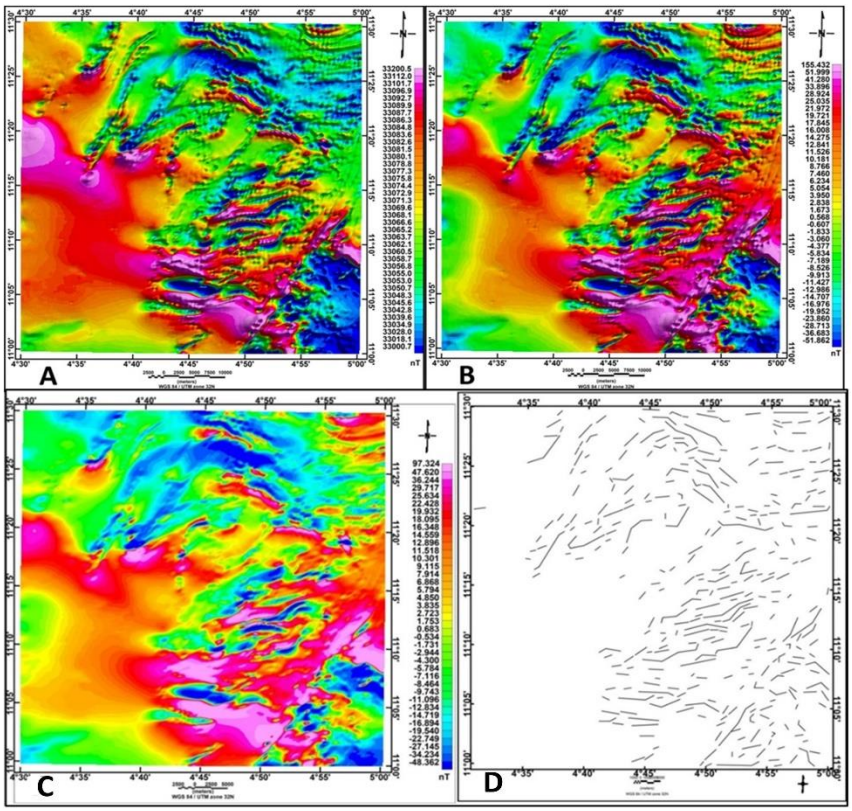

Figure 3: a. Total field map b. RMI map c. RTE map and d. represent structures delineated using the centre for exploration targeting (CET)

values vary from -51.862 nT low to 155.432 nT high. The observable differences between the RMI and the RTE map is the difference in the susceptibility ranges, the RTE susceptibility varies from -48.362 nT lowest to 97.324 nT highest as compared to the RMI map where the minimum susceptibility value is -51.862 nT low to 155.432 nT high (Figure 3b). The observed occurrence of magnetic lows and highs in figures (3a, 3b & 3c) is attributed to the effect of metasomatic alteration of magnetite and /or hydrous Fe-oxide developed in fractures that lead to the decrease in the magnetic susceptibility of the host rocks (Tawey *et al.*, 2020; Isles & Rankin, 2011). Also, Figure 3D represent the lineament map of the area automatically delineated using CET plug-In. From the lineament map, boundary between basement and sedimentary portion of the study area is established as no structure is observed within the sedimentary portion of the study area (Figure 3d).

Figure 4a represent Euler solutions with SI=1, while Figure 4b represent Euler solutions

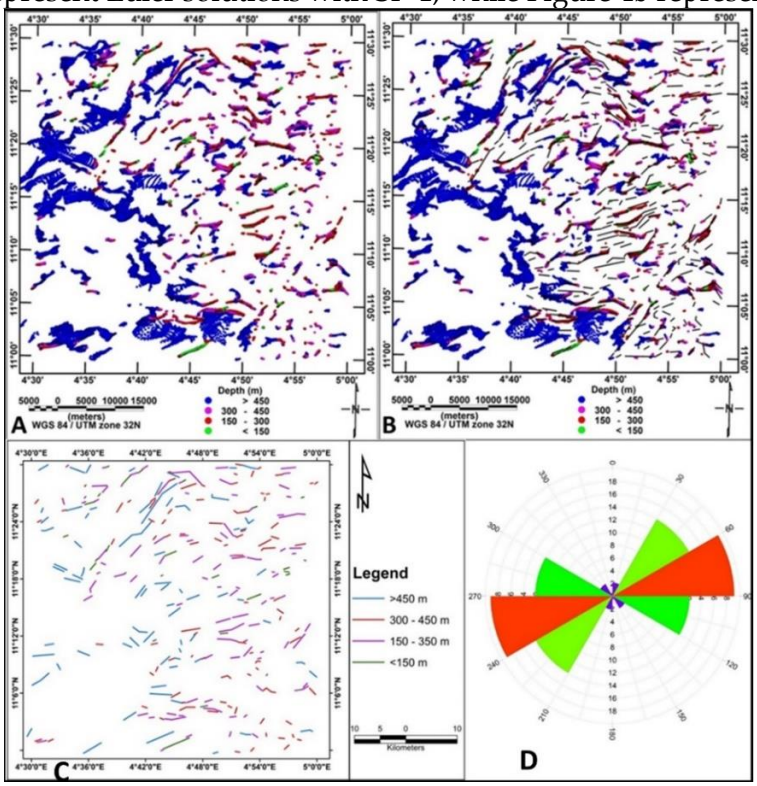

Figure 4: a. Euler Solution Map with SI=1, b. Euler Solution Map with SI=1, Overlaid with Structures delineated using the Centre for Exploration Targeting (CET), c. Classified structures with depth from 3D Euler Deconvolution (SI=1) and d. Rose Diagram

with SI=1 overlaid with CET delineated structures. Also, Figure 4c represent the delineated structures from CET overlay with Euler deconvolution with SI=1, while Figure 4d represent Rose diagram of the delineated structures. From the map (Figure 4b) most of the CET structures are seen to correlate in position and trends with structures on the Euler deconvolution map with SI=1, which invariably imply that the CET structural map is the representation of all the structures within the study area without depths, but we have been able to assign depths ranges to the delineated structures as revealed by the 3D Euler solutions map with structural index of one (Figure 4c). The statistical analysis of the delineated structures using a Rose diagram (Figure 4d) revealed the area to have been affected by tectonic activities with predominant trend of east-north-east to west-south west (ENE-WSW) followed by northeast to southwest (NE-SW), west-north-west to east-south-east (WNW-ESE), northwest to southeast (NW-SE), and north-north-east to south-south-west (NNE-SSW) in

confirmation with earlier work attributing these tectonic activities to the Pan African (Tawey & Magaji, 2022; Tawey *et al*., 2020; Andrew *et al*., 2018; Ajakaiye *et al*., 1982).

CONCLUSION

The CET approach of identifying magnetic structures assisted in elucidating the overall geological structural framework of the research area. These structures are similar in trends and position just like the structures delineated using Euler solutions with SI=1. One good characteristic of using Euler deconvolution solutions is that it enables delineation of geologic structural features of a research area with specific ranges of depth attached and this also enables one to look at a particular geologic structure in place and talk of its depth of occurrence.

REFERENCES

Abba, S.I. (1983). The structure and petrography of alkaline rocks of the Mada Younger Granite Complex, Nigeria. Journal of African Earth Science, 3, 107-113.

Ajakaiye, D.E., Hall, D.H., Miller, T.W., Verherjen, P.J.T., Awad, M.B., *et al*. (1986). Aeromagnetic anomalies and tectonic trends in and around the Benue Trough Nigeria. Nature (Physical Science), 319, 582-584.

Andrew, J., Alkali, A., Salako, K. A., & Udensi, E. E. (2018). Delineating mineralisation zones within the Keffi-Abuja area using aeromagnetic data. Journal of Geography, Environment and Earth Science International, 15(3), 1-12.

Baranov, V. (1957). A new method of interpretation of aeromagnetic maps: Pseudogravimetric anomalies. Geophysics, 22, 259-283.

Bhattacharyya, B.K. (1965). Two-dimensional harmonic analysis as a tool for magnetic interpretation. Geophysics, 30, 829-857.

Black, R. (1980). Precambrian of West Episodes. Africa, 4, 3-8.

Burke, K.C., & Dewey, J.F. (1972). Orogeny in Africa. In: Dessauvagie TFJ, Whiteman AJ (eds), African geology. University of Ibadan Press, Ibadan, 583-608.

Core, D., Buckingham, A., & Belfield, S. (2009). Detailed structural analysis of magnetic data done quickly and objectively, SGEG Newsletter.

Dada, S.S. (2006). Proterozoic evolution of Nigeria. In: Oshi O (ed) The basement complex of Nigeria and its mineral resources (A Tribute to Prof. M. A. O. Rahaman). Akin Jinad and Co. Ibadan, 29-44.

Foss, C. (2011). Magnetic data Enhancement and Depth Estimation. In H. Gupta (Ed.), Encyclopedia of Earth Sciences Series, 736-746.

Gandu, A.H., Ojo, S.B., & Ajakaiye, D.E. (1986). A gravity study of the Precambrian rocks in the Malumfashi area of Kaduna State, Nigeria. Tectonophysics, 126, 181-194.

Geosoft. (2012). Manual, CET grid analysis: How to produce structural complexity map, 1-6.

Grauch, V.S.J., & Cordell, L. (1987). Limitations of determining density or magnetic boundaries from the horizontal gradient of gravity or pseudogravity data. Short note, Geophysics, 52(1), 118-121.

Gunn, P., Minty, B., & Milligan, P. (1997). The Airborne Gamma-Ray Spectrometric Response over Arid Australian Terranes. In A. Gubins (Ed.), Proceedings of Exploration 97: Fourth Decennial International Conference on Mineral Exploration, (pp. 733-740). Australia.

Holden, E.J., Dentith, M., & Kovesi, P. (2008). Towards the automatic analysis of regional aeromagnetic data to identify regions prospective for gold deposits, Computers & Geosciences, 34(11), 1505-1513.

Isles, D. D., & Rankin, L. R. (2011). Geological interpretation and structural analysis of aeromagnetic data. TGT Consulting / Geointerp Unpublished workshop manual.

Kogbe, C.A. (1979). Geology of the Southeastern (Sokoto) sector of the Iullemeden Basin. Bulletin. Department of Geology, Ahmadu Bello University, 2(1), 91-237.

Kogbe, C.A. (1981). Cretaceous and Tertiary of the Iullemeden Basin of Nigeria (West Africa). Cretaceous Research, 2, 129-186.

Kovesi, P. (1991). Image features from phase congruency. Videre: Journal of Computer Vision Research, 1(3), The MIT Press.

Kovesi, P. (1997). Symmetry and asymmetry from local phase. AI '97, Tenth Australian Joint Conference on Artificial Intelligence, 2-4.

Li, X. (2008). Magnetic reduction-to-the-pole at low latitudes.

McCurry, P. (1976). The Geology of the Precambrian to Lower Palaeozoic Rocks of Northern Nigeria – a Review. In Geology of Nigeria. Kogbe, C.A. (Ed.), Elizabethan Publishers, Lagos, Nigeria, 15-39.

Miller, H.G., & Singh, V. (1994). Potential field tilt - A new concept for location of potential field sources. Journal of Applied Geophysics, 32, 213-217.

NGSA. (2006). Geology and Structural Lineament Map of Nigeria.

Obaje, N.G. (2009). Geology and Mineral Resources of Nigeria, Berlin: Springer-Verlag, Heidelberg, 221.

Odebode, M.O. (2010). Sokoto Basin, NW Nigeria. A Handbook on Geology.

Olayinka, A.I. (1992). Geophysical siting of boreholes in crystalline basement areas of Africa Journal of African Earth Science, 14, 197-207.

Phillips, J.D. (2000). Locating magnetic contacts: a comparison of the horizontal gradient, analytic signal, and local wavenumber methods. SEG technical program expanded abstract, 402-405.

Reid, A.B., Allsop, J.M., Granser, H., Millet, A.J., & Somerton, I.W. (1990). Magnetic interpretation in three dimensions using Euler deconvolution. Geophysics, 55, 80-91.

Reynolds, J.M. (1997). An introduction to Applied and Environmental Geophysics, John Wiley & Ltd. Bans Lane, Chichester, 124-132.

Roest, W., Verhoef, J., & Pilkington, M. (1992). Magnetic interpretation using 3-D analytic signal. Geophysics, 57, 116-125.

Tawey, M. D., & Magaji, S. S. (2022). Geology of the area around Geshare town (Kerku Ring Complex), part of sheet 146, Geshare southeast. Nigerian Journal of Water Resources, 8(1), 142-153.

Tawey, M. D., Alhassan, D. U., Adetona, A. A., Salako, K. A., Rafiu, A. A., & Udesi, E. E. (2020). Application of Aeromagnetic Data to Assess the Structures and Solid Mineral Potentials in Part of North Central Nigeria. Journal of Geography, Environment and Earth Science International, 24(5), 11-29.

Telford, W.M., Geldart, L.P., Sheriff, R.E., & Keys, D.A. (1990). Applied Geophysics. 2nd Edition, Cambridge University Press, Cambridge, 770.

Thompson, D.T. (1982). EUlDPH: A New Technique for Making Computer-Assisted Depth Estimates from Magnetic Data. Geophysics, 47, 31-37.

Verduzco, B., Fairhead, J.D., Green, C.M., & MacKenzie, C. (2004). New Insights into Magnetic Derivatives for Structural Mapping. The Leading Edge, 23, 116-119.